Comparison between High and Low Strain-Rate Deformation of Tantalum

RAJEEV KAPOOR and SIA NEMAT-NASSER

To understand the constitutive behavior of tantalum, compression tests are performed over the range of strain rates from 0.0001/s to 3000/s, and at temperatures from 296 to 1000 K. The flow stress is seen to be representable as the sum of a thermal, an athermal, and a viscous drag component. At high strain rates (3000/s), the thermal component is observed to be expressible in terms of the temperature and the strain rate, whereas the athermal component is independent of these variables. At lower strain rates, however, such a separation of the effects of the strain, strain rate, and temperature on the flow stress is not easily achieved. At high enough temperatures, *i.e.*, temperatures above which the thermal component is essentially zero, viscous drag appears to have a significant effect on the flow stress.

I. INTRODUCTION

THE mechanical properties of a material depend on its internal microstructure, and changes in these mechanical properties result from corresponding changes in the microstructure. In most materials, the microstructure continuously changes during deformation, causing the stress required for further deformation to change. This, in turn, results in work hardening. The microstructure here refers to the grain size, distribution of second-phase particles or precipitates, and distribution and density of dislocations. One common microstructure parameter used is the dislocation density. With dislocation density as the microstructural parameter, the shear stress on a slip plane can be written as

$$\tau = \tau(\rho, \dot{\gamma}, T) \qquad [1]$$

where ρ is the dislocation density, $\dot{\gamma}$ is the shear strain rate on that slip plane, and T is the temperature. The stress required to overcome a given microstructure at 0 K, referred to as the mechanical threshold stress, can also be used as a microstructural parameter.[1,2] The microstructure can evolve differently for different loading conditions, that is, for different values of $\dot{\gamma}$ and T. This results in different flow stresses at different $\dot{\gamma}$ (or T) at a given strain. Strain is not a state variable, and the variation of the stress with strain only has meaning if the initial microstructure at 0 strain is known, and there is a concurrent knowledge of microstructure evolution as a function of strain path. Previous researchers have attempted to describe the flow stress of materials using the concept of dislocation density as a microstructural parameter.[1,3–7]

The resistance to deformation can be due to: (1) dislocations overcoming periodic lattice potentials; (2) dislocations interacting with other dislocations; (3) dislocations interacting with solute atoms; (4) dislocations overcoming the long-range elastic stress field caused by grain boundaries, precipitates, dislocation forests, and other defects; and (5) dislocations overcoming the viscous drag, in the course of their motion. A moving dislocation encounters some or all of these obstacles. Obstacles that can be overcome with assistance from thermal energy are called thermal (short-range) barriers. Obstacles that cannot be overcome by thermal energy are called athermal (long-range) barriers. Viscous drag may be present depending on the temperature and stress conditions existing within the material. The total resistance to deformation may then be considered as the sum of these:

$$\tau = \tau_a + \tau^* + \tau_d \qquad [2]$$

where τ_a is the athermal resistance, τ^* is the thermal resistance, and τ_d is the resistance due to viscous drag. The athermal barriers depend on the microstructure of the material, *e.g.*, dislocation density, grain size, and precipitates. A particular microstructure may or may not evolve with deformation. For example, the dislocation density ρ evolves with the deformation, the grain size may evolve with the deformation (dynamic recrystallization), whereas precipitates and solute atoms do not evolve with the deformation, although they may rearrange their distribution through a diffusion process. Thus, the athermal stress can be separated into two components: that which evolves with deformation, τ_{a_1}, and that which remains constant with deformation, τ_{a_2}; *i.e.*,

$$\tau_a = \tau_{a_1}(\rho) + \tau_{a_2} \qquad [3]$$

There is an inherent temperature dependence in the flow stress, that of the temperature dependence of the shear modulus $\mu(T)$. The temperature dependence of μ is given as[8]

$$f(T) = \frac{\mu(T)}{\mu_0} = 1 - \frac{c_1}{\exp_T^{c_2} - 1} \qquad [4]$$

where c_1 and c_2 are empirical constants. The preceding equation can be written as $\mu(T)/\mu_0 = f(T)$, where $f(T)$ is the right side of Eq. [4]. Thus, to obtain the temperature-dependent part of the flow stress without taking into account the shear modulus dependence on the temperature, $\tau/f(T)$ instead of τ should be considered.

RAJEEV KAPOOR, Visiting Scientist, Bhabha Atomic Research Centre, Mumbai, India 40085, was formerly with the Center of Excellence for Advanced Materials, University of California, San Diego. SIA NEMAT-NASSER, Professor, is with the Center of Excellence for Advanced Materials, University of California, San Diego, La Jolla, CA 92093-0416.

This article is based on a presentation given in the symposium entitled "Dynamic Behavior of Materials—Part II," held during the 1998 Fall TMS/ASM Meeting and Materials Week, October 11–15, 1998, in Rosemont, Illinois, under the auspices of the TMS Mechanical Metallurgy and the ASM Flow and Fracture Committees.

In order to obtain a relation between $\dot{\gamma}$, T, and τ^*, a relation between ΔG (the activation free energy for overcoming a short-range barrier) and τ^* is required. Kocks *et al.*[9] suggested an empirical relation between ΔG and τ^*, representing a typical barrier encountered by a dislocation. They suggest

$$\Delta G = F_0 \left[1 - \left(\frac{\tau^* \mu_0}{\tau^* \mu(T)} \right)^p \right]^q \qquad [5]$$

where $0 < p \leq 1$ and $1 \leq q \leq 2$. Here, τ^* is the shear stress required to overcome the barrier at 0 K, and F_0 is the free energy required to overcome the barrier when the applied τ^* is zero. The term $\dot{\gamma}$ is related to ΔG as

$$\dot{\gamma} = \dot{\gamma}_0 \exp\left(-\frac{\Delta G}{kT} \right) \qquad [6]$$

where $\dot{\gamma}_0 = \rho_m \mathbf{b} a \nu$, in which ρ_m is the mobile dislocation density, **b** is the magnitude of the Burgers vector, a is the distance the dislocation moves while overcoming the obstacle, and ν is the attempt frequency. Putting Eq. [6] into [5] and simplifying, we obtain

$$\tau^* = \hat{\tau}^* \left[1 - \left(\frac{kT}{F_0} \ln \frac{\dot{\gamma}_0}{\dot{\gamma}} \right)^{1/q} \right]^{1/p} \qquad [7]$$

The total shear stress can be written as

$$\tau = \tau_{a_1}(\rho) + \tau_{a_2} + \hat{\tau}^* \left[1 - \left(\frac{kT}{F_0} \ln \frac{\dot{\gamma}_0}{\dot{\gamma}} \right)^{1/q} \right]^{1/p} + \tau_{\text{drag}} \qquad [8]$$

In the preceding analysis, shear stress τ, shear strain γ, and shear strain rate $\dot{\gamma}$ are used. It is assumed that the uniaxial stress σ, the uniaxial strain ε, and the corresponding strain rate $\dot{\varepsilon}$ are also related to each other in a manner similar to Eq. [8],

$$\sigma = \sigma_{a_1}(\rho) + \sigma_{a_2} + \hat{\sigma}^* \left[1 - \left(\frac{kT}{F_0} \ln \frac{\dot{\varepsilon}_0}{\dot{\varepsilon}} \right)^{1/q} \right]^{1/p} + \sigma_{\text{drag}} \qquad [9]$$

Zurek *et al.*[10] used similar types of equations to model tungsten and tungsten alloys. Nemat-Nasser and Isaacs[11] used this technique of splitting up the flow stress into a thermal component and an athermal component in order to model the constitutive behavior of tantalum at high strain rates.

By definition, the thermal stress component, σ^*, depends on $\dot{\varepsilon}$ and T, whereas the athermal stress component, σ_a, depends on the microstructure, which in turn depends on the deformation (effective strain). Depending on the deformation mechanisms, σ_a may also depend on the $\dot{\varepsilon}$ and the T histories, and σ^* may also depend on the microstructure. Nemat-Nasser and Li[12] modeled the constitutive behavior of copper at high strain rates, with σ^* not only depending on $\dot{\varepsilon}$ and T but also depending on average dislocation spacing and hence on the average density of the dislocations, ρ. These authors take ρ to be a function of strain, here ε, for a given deformation path; note that, for the general three-dimensional case, ε is the effective strain, a monotonically increasing quantity. Also, Follansbee and Kocks[1] explored the dependence of σ^* on the strain path. These dependences can be verified by strain-rate-change and temperature-change experiments. In order to check the dependence of σ^* on $\rho(\varepsilon)$, strain-rate-change tests can be carried out at various strains. During a sudden change in the strain rate or the temperature, the microstructure of the material remains essentially unchanged.* Because σ_a depends only on the microstructure, it should not change with a sudden change in either $\dot{\varepsilon}$ or T. On the other hand, the part that would certainly change is σ^*. In other words, the change in σ due to a change in $\dot{\varepsilon}$, at a given strain, is due to a change in σ^*, provided that the viscous drag can be neglected, which is discussed later in Section IV. Figure 1 is a schematic diagram depicting a change of the strain rate at different strain values. The change in the stress is due to a change, $\Delta\sigma^*$, in the thermal component. Thus, by only changing $\dot{\varepsilon}$ at different ε values, $\Delta\sigma^*$ as a function of $\rho(\varepsilon)$, and hence a function of ε, can be obtained. In order to check the dependence of σ_a on ε and T, either strain-rate-change tests or temperature-change tests need to be carried out. Figure 2 shows two types of responses: (a) the case when the microstructure of the material does not evolve differently at different strain rates, and (b) the case when the microstructure of the material evolves differently at different strain rates. In case (a), if the strain rate is changed at point P from ε_1 to ε_2, the flow stress will jump to the value at point Q and follow the flow stress of the sample deformed from the start at ε_2. On the other hand, in case (b), if the strain rate is changed at point P, the flow stress jumps to point Q', beyond which the work-hardening rate is different from the work-hardening rate for the test at ε_1. Thus, by performing strain-rate-change tests and temperature-change tests, the dependence of σ_a on ε and T can be determined. Likewise, the dependence of σ^* on ε (through the dependence of ρ on ε) can be determined.

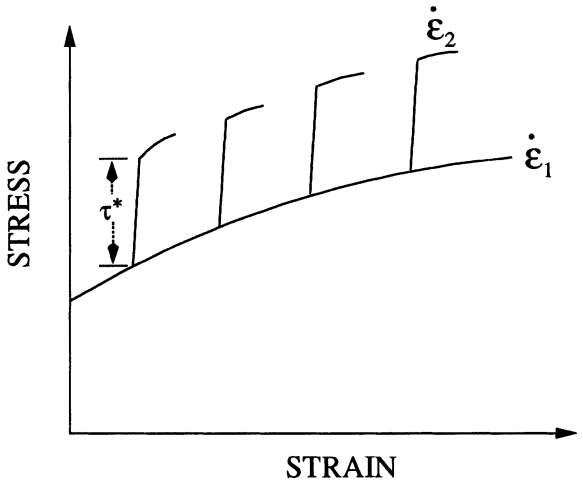

Fig. 1—Schematic diagram depicting change of flow stress arising from change of strain rate at different strain values.

Cottrell and Stokes[13] used temperature-change tests to determine the effect of the microstructural evolution on the temperature sensitivity of the flow stress. From experiments carried out on aluminum, they concluded that $\Delta\sigma$ is proportional to σ, where $\Delta\sigma$ is the change in the flow stress caused by a sudden change in the temperature, at a constant strain rate. For the case of iron, $\Delta\sigma$ is independent of the strain.[14]

*It is difficult to experimentally perform rapid temperature-change tests. During the process of heating the sample from one temperature to the other, it is possible that some recovery may occur. In the present set of experiments, no such recovery was observed.

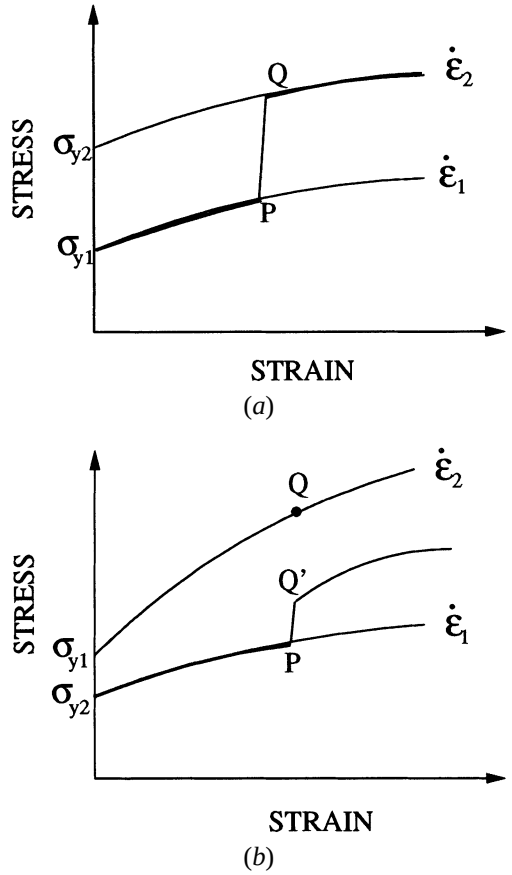

Fig. 2—Schematic diagram depicting change of strain-rate tests for (*a*) material whose microstructure does not evolve differently at different strain rates and (*b*) material whose microstructure evolves differently at different strain rates.

Klepaczko[15] and Klepaczko and Chiem[16] carried out strain-rate-change tests on fcc metals in order to determine the effect of the deformation history on the strain-rate sensitivity of the flow stress, as well as on strain hardening. Hoge and Mukherjee[17] carried out experiments on tantalum over a range of strain rates and temperatures and concluded that the rate-controlling mechanism associated with the yield stress is the Peierls mechanism. Meyers *et al.*[18] and Chen *et al.*[19] noted a parallel shift of the true stress-strain curve with a change in the strain rate. Steinberg and Lund[20] formulated a constitutive model separating the yield stress into athermal and thermal components, with the work hardening term being a part of the athermal term. Instantaneous strain-rate-change tests also resulted in the same flow stress as would have resulted if the material were deformed only at the second strain rate. These results suggest that the internal microstructure of the considered material did not depend on the strain rate. Gray and Vecchio[21] studied the effect of shock loading on Ta and Ta-10%W alloy (pressures of 7 and 20 GPa). They observed no enhanced shock hardening as compared to quasi-static or dynamic deformations, suggesting that microstructural evolution does not depend on the loading conditions. Lopatin *et al.*[22] compared the higher strain rate *vs* lower strain rate response in tantalum, and carried out experiments to determine whether properties of tantalum depend on the deformation path. Strain-rate-change tests were carried out from higher strain rates to lower strain rates, and a strain-rate path dependence was observed. It was suggested that different dislocation microstructures are produced during different strain-rate loading histories. Thus, there are conflicting experimental data regarding the strain-path dependence of work hardening.

The objective of the present research is to experimentally determine the validity of separating the uniaxial flow stress σ only into a thermal component σ^* and an athermal component σ_a, neglecting viscous drag for the case of commercially pure tantalum. In the simplest of cases, σ^* only depends on the applied ε and T, and σ_a only depends on $\rho(\varepsilon)$, and hence ε (for a given deformation path). Apart from this, does σ^* also depend on the strain path? Does σ_a depend on the history of deformation (applied ε and T)? If so, then in what range are these conditions valid? Is there a drag effect on the motion of dislocations? These are the questions this article attempts to answer.

II. EXPERIMENTAL PROCEDURE

Commercially pure tantalum, obtained in the form of disks from the U.S. Army Ardec, was used in the present study. The material was originally in the form of 41-mm-diameter bars. These were cold upset forged to 19-mm-high barrels and annealed. These were high-energy-rate formed to a liner roughly 5-mm thick and were then annealed. The tantalum had a grain size of about 85 μm. There was no observable difference in the grain size between the two orthogonal directions of the disk. The major impurities present were C $\approx$ 10 ppm, O $\approx$ 60 ppm, N $\approx$ 10 ppm, Si $\approx$ 10 ppm, and Nb $\approx$ 60 ppm.

Compression tests were carried out on Ta at strain rates ranging from 10^{-4}/s to 3000/s and temperatures ranging from 296 to 1000 K. Strain rates of 10^{-4}/s to 1/s were achieved in a hydraulic Instron machine, whereas strain rates of 300/s and higher were achieved using a Hopkinson bar. Isothermal compression tests at 3000/s and 296 K were also carried out. High-temperature deformation tests at low strain rates were carried out using a radiant furnace, with argon flowing through the furnace to prevent excess oxidation of the sample surface. Alumina push rods were used as a means of compressing samples in the furnace. The strain was measured by using the LVDT (Linear Variable Differential Transformer) signal and subtracting out the displacement of the load train setup.

Strain rates of 300/s and higher were achieved using a split Hopkinson pressure bar with a momentum trap.[23–26] In order to carry out high-temperature tests using the Hopkinson bar, the apparatus was modified, such that minimal heating of the incident and transmission bars took place; for more details, see Nemat-Nasser and Isaacs.[11] In order to better understand the microstructural evolution of Ta, strain-rate-change tests as well as temperature-change tests were performed.

III. RESULTS

A. *High Strain-Rate Results*

During adiabatic deformation at a constant strain rate, it is assumed that the change in the flow stress is due to (1) change in the strain (used as an independent variable) and (2) change in the temperature; *i.e.*,

$$d\sigma = \frac{\partial \sigma}{\partial \varepsilon} d\varepsilon + \frac{\partial \sigma}{\partial T} dT \quad [10]$$

$$\frac{d\sigma}{d\varepsilon} = \frac{\partial \sigma}{\partial \varepsilon} + \frac{\partial \sigma}{\partial T} \frac{dT}{d\varepsilon} \quad [11]$$

From the adiabatic stress-strain curves, $d\sigma/d\varepsilon$ can be obtained, but actually $\partial\sigma/\partial\varepsilon$ is the isothermal work hardening rate, *i.e.*, the work hardening rate devoid of any temperature rise during deformation. In order to obtain $\partial\sigma/\partial\varepsilon$, both $\partial\sigma/\partial T$ and $dT/d\varepsilon$ need to be determined. In order to calculate $dT/d\varepsilon$, it is assumed that within experimental error all the work of deformation is converted to heat.[11,27] The heat generated results in a temperature rise of the material. If $\sigma d\varepsilon$ is the work done on the material in the strain increment of $d\varepsilon$, and dT is the corresponding rise in temperature, then

$$\sigma d\varepsilon = \lambda C_v dT \quad [12]$$

$$\frac{dT}{d\varepsilon} = \frac{\sigma}{\lambda C_v} \quad [13]$$

Here, λ is the density of the material, and C_v is specific heat at constant volume. Putting Eq. [13] in Eq. [11], we obtain

$$\frac{\partial \sigma}{\partial \varepsilon} = \frac{d\sigma}{d\varepsilon} - \frac{\partial \sigma}{\partial T}(\varepsilon, T) \frac{\sigma}{\lambda C_v} \quad [14]$$

Integration of Eq. [14] with respect to ε gives

$$\sigma_{\text{iso}} = \sigma_{\text{adbt}} - \int \frac{\sigma}{\lambda C_v} \frac{\partial \sigma}{\partial T}(\varepsilon, T)\, d\varepsilon \quad [15]$$

By knowing the variation of σ with T, $(\partial\sigma/\partial T)$, as a function of ε, the preceding integral can be calculated. If $\partial\sigma/\partial T$ is a function only of T and not of ε, the calculation becomes simple.

There is an experimental technique for determining the isothermal flow stress at various temperatures, developed by Nemat-Nasser *et al.*[28] In this technique, the deformation is carried out in steps. A sample is deformed to a strain, say, 0.1, and then unloaded, and its temperature is brought back to the original loading temperature. The sample is then reloaded at the original temperature, again to a similar strain increment (0.1 in this case), at the same strain rate. This step is repeated until the desired total strain is attained. The reload flow stresses represent stresses at the original temperature of loading. These points can then be connected in a smooth manner to obtain an isothermal stress-strain curve. Ideally, a true isothermal stress will be obtained only if the true strain increments approach zero. However, this is not possible, and finite strain increments need to be considered, from which only about four or five isothermal stress points can be obtained. These results can then be augmented by overlapping with additional incremental tests. The advantage of this experimental method is that the isothermal stress can be obtained without having to know the temperature-sensitivity of the stress $(\partial\sigma/\partial T)$. It is useful to obtain isothermal flow stress curves for high strain-rate tests, because the effect of an increase of the temperature during deformation on the flow stress can be eliminated. The work hardening rate obtained using an isothermal flow stress is only due to the evolution of the microstructure during deformation, and not due to a deformation-induced change in the temperature.

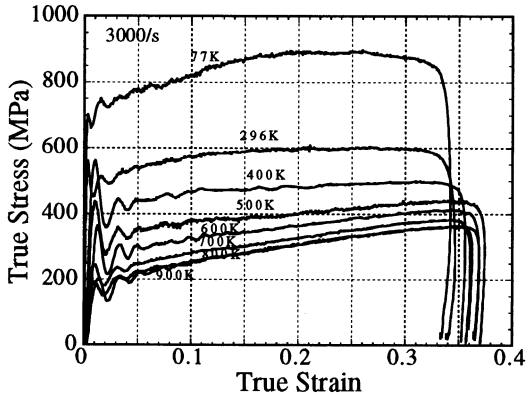

(*a*)

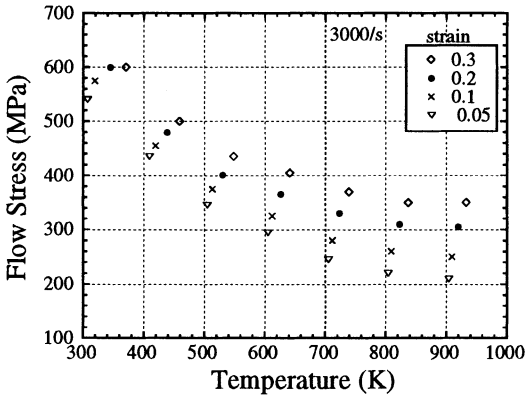

(*b*)

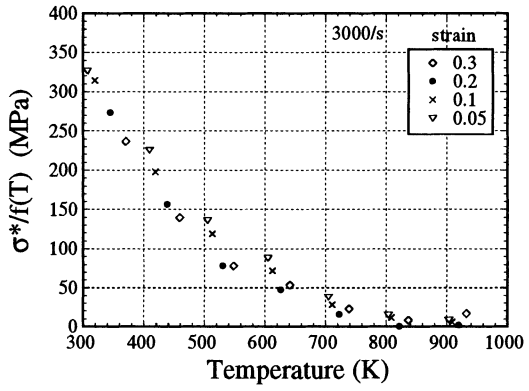

(*c*)

Fig. 3—(*a*) Flow stress curves for Ta deformed at 3000/s; (*b*) flow stress for Ta as a function of temperature at different strains; and (*c*) $\sigma^*/f(T)$ as a function of temperature for different strain values.

Figure 3(a) shows stress-strain curves for Ta tested at 3000/s at various indicated initial temperatures.* In order to calculate the isothermal stress, the variation of σ with T as a function of ε must be established. Figure 3(b) is a plot of the flow stress as a function of the temperature at different strains. The flow stress decreases with an increase in the temperature up to a point where the flow stress becomes nearly independent of the temperature. It is assumed that when σ becomes independent of T, it represents the athermal stress component, σ_a. This value (σ_a) can be subtracted from

*The temperatures mentioned in the diagram are the initial temperatures. The sample temperature increases due to the adiabatic nature of the tests.

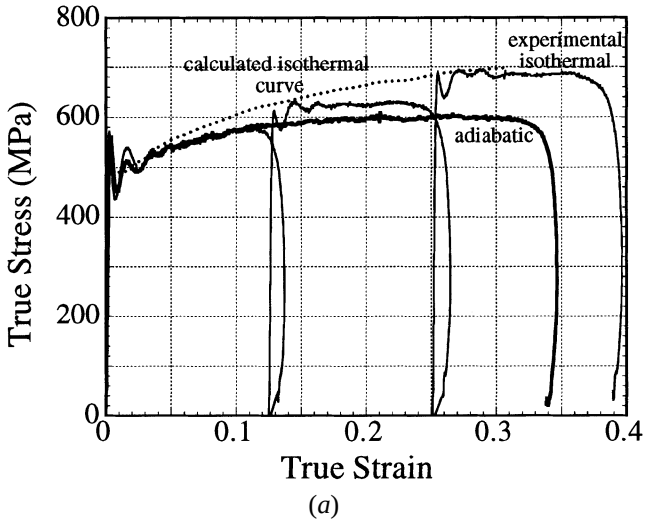

(*a*)

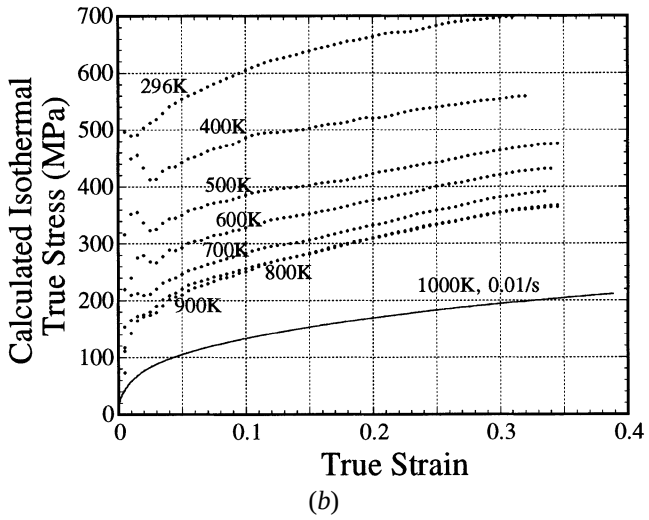

(*b*)

Fig. 4—(*a*) Comparison of calculated isothermal stress for Ta and experimentally obtained isothermal data points; (*b*) Calculated isothermal curves at 3000/s for Ta. The last curve is at 1000 K and 0.01/s and is placed here for comparison.

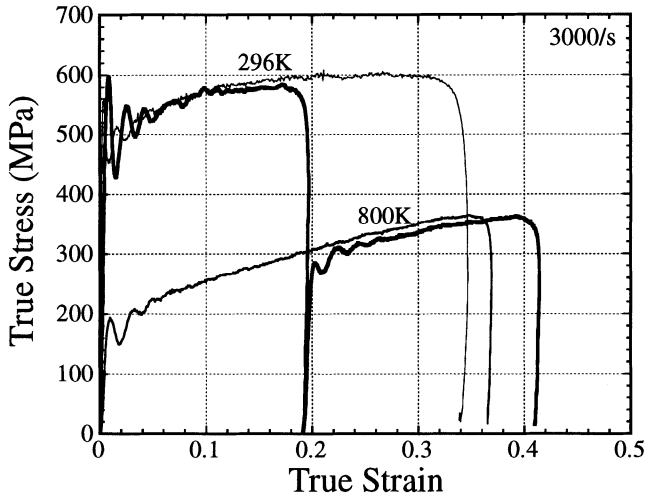

Fig. 5—Temperature-change test from 296 to 800 K, carried out on tantalum at a strain rate of 3000/s.

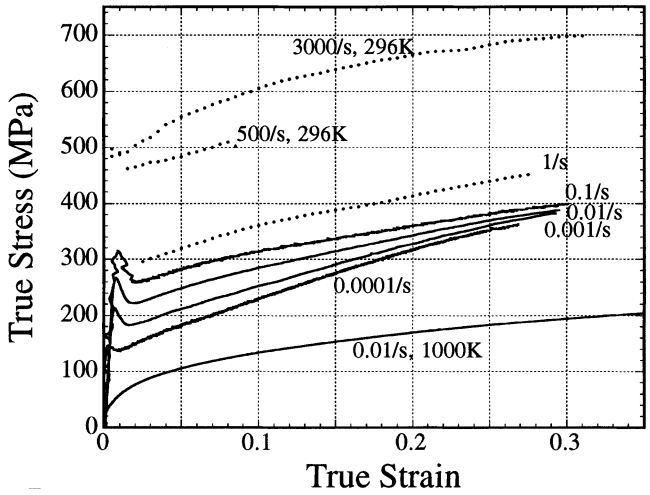

Fig. 6—Flow stress curves at 296 K at different strain rates.

the overall stress σ to obtain the thermal component of the stress, σ^*. As seen in Figure 3(c), the σ^* values for different strains approximately fall on the same curve, indicating that in this strain-rate and temperature range, $\partial\sigma/\partial T$ does not depend on ε. Using Eq. [15], the corresponding isothermal stress as a function of the strain can be obtained. In Figure 4(a) is shown the calculated isothermal flow stress as well as the incremental strain tests performed to simulate the isothermal testing conditions. The calculated isothermal flow stress curve does pass through the reload yield stress points obtained from the incremental strain tests. Figure 4(b) shows the calculated isothermal flow stress for higher-temperature deformations. Also shown in Figure 4(b) is the flow stress curve for Ta deformed at 1000 K and 0.01/s. It is assumed here that this curve (1000 K–0.01/s) represents the athermal flow stress in Ta. At this strain rate of 3000/s, the resulting isothermal stress-strain curves are parallel to each other; *i.e.*, they are only shifted along the stress axis.

In order to verify the temperature dependence of the microstructural evolution at a strain rate of 3000/s, temperature-change tests were carried out. One sample was tested at 296 K and 3000/s up to a strain of 0.2, unloaded, and then reloaded at 820 K and 3000/s. The reloading temperature was 820 K and not 800 K, because that was the temperature reached after a strain of 0.22, from an initial temperature of 800 K, due to adiabatic heating. As seen in Figure 5, the reload stress matched the flow stress of the sample continuously loaded at an initial temperature of 800 K and at a strain rate of 3000/s. This implies that in this temperature and strain-rate range, the strain term (actually, the dislocation density term) is decoupled from the strain rate and the temperature term. The flow stress can be separated into an athermal stress and a thermal stress such that the athermal stress is independent of the strain rate and the temperature, whereas the thermal stress is independent of the deformation history. The macroscopic stress can thus be written as

$$\sigma(\varepsilon,\dot{\varepsilon},T) = \sigma_a(\varepsilon) + \sigma^*(\dot{\varepsilon},T) \qquad [16]$$

B. *Room-Temperature Deformation at Different Strain Rates*

Results of compression tests carried out on Ta at different strain rates (0.0001/s to 3000/s) are shown in Figure 6. It

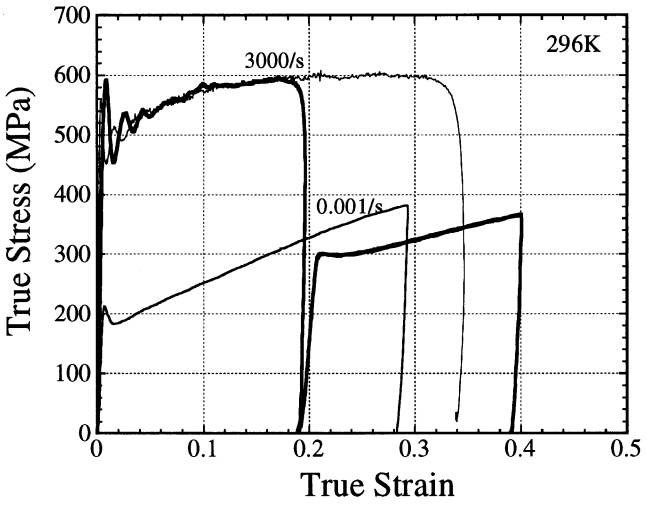

Fig. 7—Strain-rate-change tests from 3000/s to 0.001/s, deformed at 296 K.

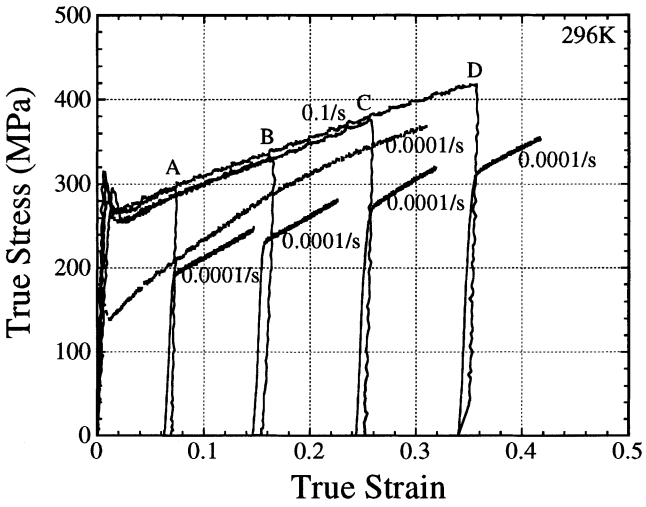

Fig. 8—Strain-rate-change tests at room temperature, for different values of strain. Strain rate was changed from 0.1/s to 0.0001/s

was noted that the deformation at a strain rate of 1/s was essentially adiabatic. The adiabatic flow stress obtained was converted to an isothermal flow stress by the procedure mentioned previously. Also shown in Figure 6 is the isothermal flow stress for Ta deformed at strain rates of 500/s and 3000/s. Although flow stresses above a strain rate of 0.1/s may be considered parallel to each other, the flow stresses below a strain rate of 0.1/s certainly are not. The work hardening rate appears to increase as the strain rate decreases. This suggests that the microstructure may be evolving differently at lower strain rates as compared to higher strain rates. At the point of instantaneous change in the strain rate, the microstructure of the material remains unchanged. Because σ_a depends only on the microstructure, it does not change with instantaneous changes in ε or T, and the only part that changes is σ^*. Let $\Delta\sigma_{\text{inst}} = \sigma_{3000/s} - \sigma_{0.001/s}$ be the instantaneous stress change, and let $\Delta\sigma = \sigma_{3000/s} - \sigma_{0.001/s}$ be the stress difference at a given strain, for samples deformed separately. Then, $\Delta\sigma = \Delta\sigma_{\text{inst}}$ implies that σ_a does not change with the strain-rate history. On the other hand, if $\Delta\sigma$ is different from $\Delta\sigma_{\text{inst}}$, then σ_a does change with the strain-rate history. If $\Delta\sigma = \Delta\sigma_y$, then σ^* does not change with ε, where $\Delta\sigma_y$ is the difference in the yield stress at 3000/s and 0.001/s. Thus, in order to verify whether σ_a depends on the strain-rate history, a strain-rate-change test was carried out at room temperature. One sample was deformed at 296 K and 3000/s up to a strain of 0.2, unloaded, and reloaded at 296 K and 0.001/s. Figure 7 shows this experimental result. The reload flow stress is lower than the flow stress of the sample continuously loaded at 0.001/s–296 K. This suggests that in this temperature regime, σ_a does change with ε. This change of the athermal stress with the strain-rate history suggests that at this temperature the microstructural evolution depends on the history of the applied strain rate.

In Figure 6, it is seen that at lower strain rates, as the strain rate decreases, the work hardening rate increases. There is a striking difference in the work hardening rate for samples deformed at 0.1/s as compared to those deformed at 0.0001/s. This difference can be either due to the change in σ_a with deformation or due to the change in σ^* with deformation. One way to determine this is to carry out a change-of-strain-rate test from 0.1/s to 0.0001/s at different strain values.

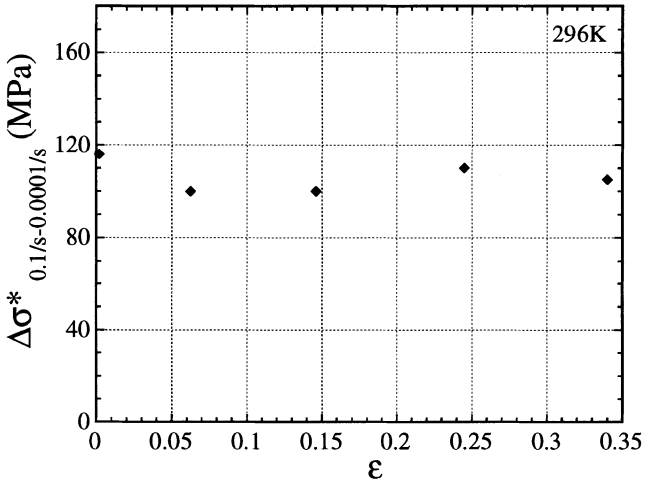

Fig. 9—Difference in the thermal component of stress corresponding to a change in strain rate from 0.1/s to 0.0001/s, as a function of strain.

Since a change in ε at constant ε only changes σ^*, a change in ε at different values of ε will determine how $\Delta\sigma^*$ varies with ε. Figure 8 is a plot of the result of this experiment. Tantalum samples were loaded at 0.1/s and 296 K up to various strain levels (yield strain, 0.065, 0.146, 0.245, and 0.34). Each of these samples was then reloaded at 0.0001/s and 296 K. Also shown in Figure 8 is tantalum deformed from the start at 0.0001/s. For each of the strain values, the reload stress does not match the flow stress of the sample deformed from the start at 0.0001/s. The difference in the reload stress between 0.1/s and 0.0001/s represents the corresponding difference in σ^*. A plot of this stress difference ($\Delta\sigma^*_{0.1/s-0.0001/s}$) as a function of ε, is shown in Figure 9. Within experimental error, $\Delta\sigma^*$ does not depend on ε, which confirms the view that σ^* does not depend on the extent of deformation.

IV. DISCUSSION

The temperature sensitivity of the flow stress at 3000/s is independent of the strain. At this high strain rate, the

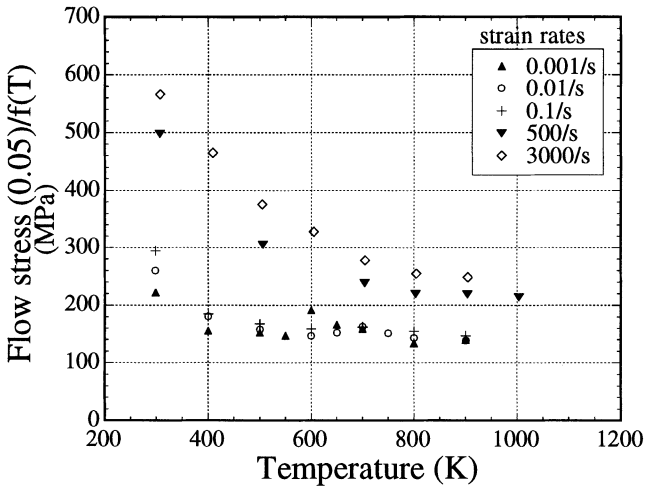

Fig. 10—Flow stress (0.05 strain) of Ta as a function of temperature, at different strain rates.

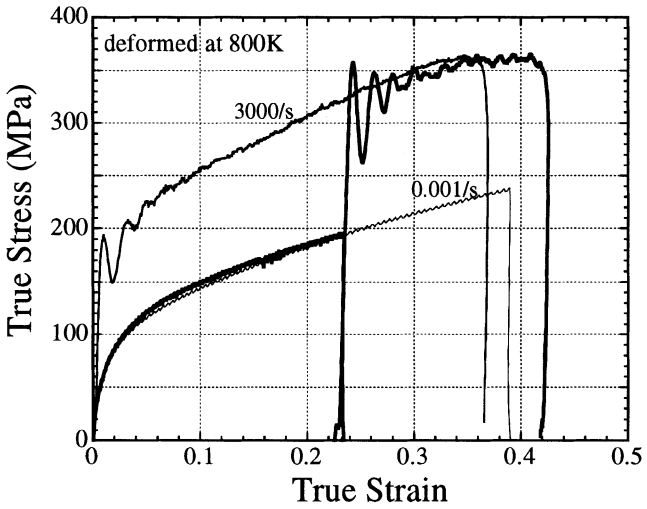

Fig. 11—Change of strain rate from 10^{-3}/s to 3000/s, deformed at 800 K.

isothermal flow stresses at different temperatures are similar and are only shifted parallel to each other. The flow stress is assumed to be a sum of two parts: one part σ^*, being a function of only the strain rate and temperature, ε and T; and the other part, σ_a, being a function of only the microstructure, here approximately represented by strain, ε. Although plastic strain cannot be a state variable, here it is used as an independent variable. At lower strain rates (0.1/s to 0.0001/s), on the other hand, the work hardening rate varies with ε and T. Thus, unlike at high strain rates, at lower strain rates, the flow stress cannot be separated into a strain-dependent term and a strain-rate/temperature-dependent term. Thus, either σ^* has a ε dependence or σ_a has a ε, T-history dependence. The strain-rate-change tests, as shown in Figure 8, help to clarify this. A plot of $\Delta\sigma^*$ as a function of ε (Figure 9) suggests that $\Delta\sigma^*$, and hence σ^*, does not depend on ε. This suggests that the difference in the work hardening behavior is due to the difference in the long-range barriers rather than a change in the short-range barriers to be overcome by dislocations. In other words, the short-range barriers are not affected by the evolving microstructure.

Figure 10 is a plot of $\sigma/f(T)$ *vs* T at a 0.05 strain and different strain rates. As observed in this figure, for each of the strain rates, a limiting temperature exists above which $\sigma/f(T)$ no longer depends on the temperature. In the case where the flow stress can be separated into σ^*, σ_a, and σ_{drag}, the flow stress will decrease with increasing temperature, until a critical temperature T_c is reached, above which $\sigma^* = 0$. Beyond T_c, at a given strain rate, the flow stress remains constant. From Eq. [9], the critical temperature is obtained from

$$\left[1 - \left(\frac{kT_c}{F_0} \ln \frac{\dot{\varepsilon}_0}{\dot{\varepsilon}}\right)^{1/q}\right]^{1/p} = 0 \qquad [17]$$

which yields

$$T_c = \frac{F_0}{k \ln \frac{\dot{\varepsilon}_0}{\dot{\varepsilon}}} \qquad [18]$$

As $\dot{\varepsilon}$ increases, the temperature at which σ^* vanishes, T_c, increases.

Table I. List of All the Strain-Rate-Change Tests and Temperature-Change Tests Carried Out on Tantalum

Initial Condition	Changed Condition	Reload Stress Matched?	Figure
296 K, 3000/s	800 K, 3000/s	yes	5
296 K, 3000/s	296 K, 0.001/s	no	7
800 K, 0.001/s	800 K, 3000/s	yes	11

As is seen in Figure 10, there exists a clear difference in the plateau stresses (the level at which stress is constant with temperature) at different strain rates, at a strain of 0.05. In order to verify whether this difference in the plateau stress level is due to the evolution of the microstructure, strain-rate-change tests were carried out at these higher temperatures. One sample was deformed at a strain rate of 10^{-3}/s and an initial temperature of 800 K, up to a strain of 0.22. This was then unloaded and reloaded at 3000/s at 830 K (original temperature was 800 K, but reached 830 K at 0.23 strain, due to adiabatic heating). This experimental result is shown in Figure 11. The reloaded stress matched the stress of the sample loaded directly at 3000/s and 800 K. From this, it can be concluded that the difference in the stresses at different strain rates at 800 K is not due to the difference in the athermal stresses. Such a matching up of the flow stress in a strain-rate-change test can only be attributed to a microstructure-independent type of stress component. If the difference in the flat portion of the $\sigma/f(T)-T$ curves at different strain rates were due to microstructural evolution, then on reloading, the stress would not reach that of the previous curve. The stress would have started off from its unloaded value and steadily climbed to the stress level originally attained at 3000/s. A summary of all the strain-rate-change tests and temperature-change tests is given in Table I.

Thus, during high strain rates and during low strain rates–high temperatures, microstructural evolution appears to be independent of ε and T. It is only at low strain rates and room to intermediate temperatures that the dependence of the microstructural evolution on ε and T is observed.

The stress level appears to change with ε, even at high temperatures where $\sigma^* = 0$ (Figure 10). In order to further

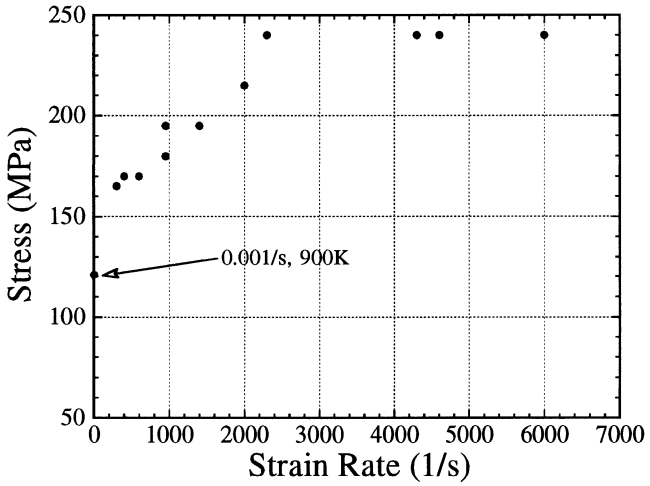

Fig. 12—Flow stress at 0.05 strain at 900 K as a function of strain rate.

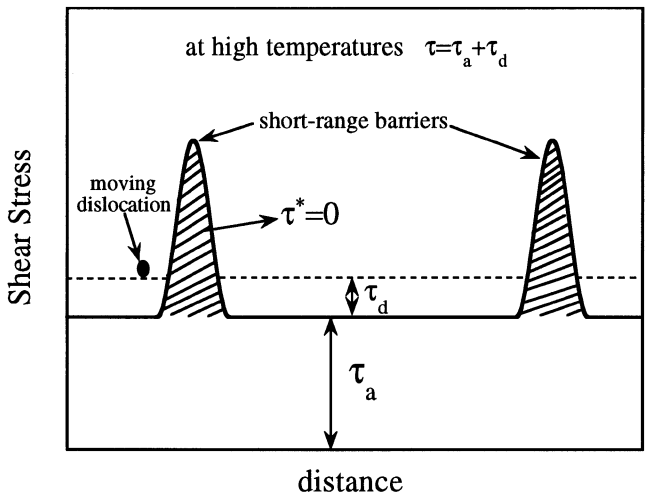

Fig. 13—Schematic representation of a dislocation moving through a long-range stress field in a crystal. The temperature is high enough such that the short-range barriers are "invisible."

investigate this strain-rate dependence at high temperatures, compression tests were carried out at 900 K at strain rates ranging from 300/s to 6000/s. The flow stress at a 0.05 strain is plotted against the strain rate in Figure 12. The flow stress increases with the strain rate up to 2300/s, after which the flow stress becomes independent of the strain rate. The data point shown by an arrow has a strain rate of 0.001/s and is plotted here for comparison with the high strain-rate data. One possible reason for the linear increase of the flow stress with the strain rate is the presence of viscous drag on the motion of dislocations. At the high temperature of 900 K, $\sigma^* = 0$, as is seen in Figure 10. Thus, dislocations gliding in a crystal are not resisted by short-range barriers. The only shear resistance they have to overcome is that due to long-range barriers, σ_a, and a drag stress associated with either phonon vibrations or solute atom drag. Figure 13 schematically shows a dislocation moving in a long-range stress field τ_a at a high temperature such that $\tau^* = 0$; τ is used for the resolved shear stress. In addition to τ_a, this dislocation experiences a viscous drag force proportional to its velocity:

$$\tau_d = \frac{Bv}{\mathbf{b}} \qquad [19]$$

where τ_d is the drag shear stress; **b** is the magnitude of the Burgers vector; v is the dislocation velocity; and B is the damping coefficient, which increases with an increase in temperature.[29] The shear strain rate, $\dot{\gamma}$, is

$$\dot{\gamma} = \rho_m b v \qquad [20]$$

where ρ_m is the mobile dislocation density. From Eqs. [19] and [20], the drag shear stress can be related to the shear strain rate as

$$\tau_d = \frac{B\dot{\gamma}}{\rho_m \mathbf{b}^2} \qquad [21]$$

For polycrystals, the macroscopic stress, σ_d, is related to the shear stress, τ_d, as $\sigma_d = M\tau_d$, where M is the average Taylor factor. The macroscopic strain rate $\dot{\varepsilon}$ may be related approximately to the shear strain rate, $\dot{\gamma}$, as $\dot{\varepsilon} = \dot{\gamma}/M$.[30] Equation [21] can now be written for the corresponding macroscopic quantities such that the drag flow stress, σ_d, is linearly related to the axial strain rate, $\dot{\varepsilon}$. Thus, in the temperature regime where $\sigma^* = 0$, the total stress can be written as

$$\sigma = \sigma_a + \frac{M^2 B}{\rho_m \mathbf{b}^2}\dot{\varepsilon} \qquad [22]$$

For bcc metals, $M \approx 2.75$.[31] In the present set of experiments at 900 K, σ does linearly increase with $\dot{\varepsilon}$ up to $\dot{\varepsilon} <$ 2000/s, suggesting that viscous drag could be the mechanism in this regime. In order to estimate the drag stress at 900 K and 2000/s, it is assumed that $B = 10^{-4}$ N s/m^2[29] and $\mathbf{b} = 3 \times 10^{-10}$ m. The estimated value of σ_d will depend on the value of ρ_m. If it is assumed that $\rho_m = 10^{11}$/m^2, then $\sigma_d =$ 170 MPa; and if $\rho_m = 10^{12}$/m^2, then $\sigma_d = 17$ MPa. The corresponding dislocation velocity, v, can be estimated from the strain rate using

$$v = \frac{M\dot{\varepsilon}}{\rho_m \mathbf{b}} \qquad [23]$$

At $\dot{\varepsilon} = 2000$/s, if $\rho_m = 10^{11}$/m^2, then $v = 195$ m/s; and if $\rho_m = 10^{12}$/m^2, then $v = 19.5$ m/s. The average velocity of the dislocations during drag starts from about 0.01 C, where C is the longitudinal wave speed.[29] For tantalum, $C = 4000$ m/s. Thus, the average dislocation velocity should be around 40 m/s. The preceding estimates imply that viscous drag may be of significance if the mobile dislocation density (at 0.05 strain) is in the range of 10^{11}/m^2 to 10^{12}/m^2. At a strain rate of 0.001/s, $\sigma_d \approx 10^{-5}$ MPa. Thus, the data point shown by the arrow in Figure 12 represents the athermal stress only. As the strain rate increases, the stress due to drag also increases ($\dot{\varepsilon} <$ 2300/s). An increase in the drag stress with strain rate occurs because of a corresponding increase in the average dislocation velocity. When the drag stress no longer increases with increasing strain rate ($\dot{\varepsilon} >$ 2300/s), the implication is that the average dislocation velocity remains essentially constant with increasing strain rate. The increase in the strain rate is then accommodated by an increase in the density of the mobile dislocations. Regazzoni *et al.*[30] have described the drag mechanism, but have considered this only when the shear stress exceeds or is in transition to exceed the mechanical threshold stress. In the present high-temperature case, the

velocity of the dislocations is no longer controlled by thermally activated processes and the only other obstacles to be overcome are long-range barriers. Thus, although the stress does not reach the mechanical threshold stress, it is likely that the dislocation experiences viscous drag, due to the simple fact that the short-range barriers are no longer present.

V. CONCLUSIONS

1. In the high strain-rate regime, the macroscopic stress can be written as the sum of a nonthermally activated deformation-dependent term and a thermally activated deformation-independent term. Temperature-change tests verify the validity of this assumption.
2. At lower strain rates (0.1/s to 0.0001/s) and high temperatures (>400 K), the macroscopic stress cannot simply be separated into a strain-dependent term and a strain-rate–temperature-dependent term.
3. Temperature-change tests carried out at low strain rates and high temperatures suggest that microstructural evolution does depend on the applied strain rate and temperature. At all the strain rates and temperatures investigated, the thermal stress component, hence, the short-range barriers, do not change with deformation and the evolution of the microstructure.
4. At high temperatures, the viscous drag mechanism makes an important contribution to the flow stress. The flow stress increases roughly linearly with the strain rate, up to a certain strain rate, beyond which it remains constant.

Thus, the flow stress can be written as

$$\sigma(\varepsilon,\dot{\varepsilon},T) = \sigma_a(\varepsilon;H(\varepsilon,\dot{\varepsilon},T)) + \sigma^*(\varepsilon,\dot{\varepsilon},T) + \sigma_{\text{drag}}(\varepsilon,\dot{\varepsilon},T) \qquad [24]$$

where $H(\ )$ represents the history dependence of the variables. The thermally activated component is dominant at low temperatures. The viscous drag component is important at high temperatures and high strain rates, in particular, when the thermally activated part vanishes.

ACKNOWLEDGMENTS

This work was supported by the Army Research Office (ARO) under Contract No. DAAH04-96-1-0376 to the University of California, San Diego.

REFERENCES

1. P.S. Follansbee and U.F. Kocks: *Acta Metall.*, 1988, vol. 36, pp. 81-93.
2. W.H. Gourdin and D. Lassila: *Tantalum. Proc. Symp. Held at 125th TMS Annual Meeting and Exhibition*, E. Chen, A. Crowson, E. Lavernia, and W. Ebihara, eds., TMS, Warrendale, PA, 1995 pp. 219-23.
3. U.F. Kocks: *J. Eng. Mater. Technol.*, 1976, vol. 98, pp. 76-85.
4. H. Mecking and U.F. Kocks: *Acta Metall.*, 1981, vol. 29, pp. 1865-75.
5. Y. Estrin and H. Mecking: *Acta Metall.*, 1984, vol. 32, pp. 57-70.
6. P.S. Follansbee, J.C. Huang, and G.T. Gray: *Acta Metall. Mater.*, 1990, vol. 38, pp. 1241-54.
7. H. Mecking and Y. Estrin: *Constitutive Relations and Their Physical Basis: Proc. 8th Riso Int. Symp. on Metallurgy and Materials Science*, S.I. Anderson, ed., Technical University Hamburg, Hamburg, 1990 pp. 123-45.
8. G. Simmons and H. Wang: *Single Crystal Elastic Constants and Calculated Aggregate Properties: A Handbook*, 2nd ed. The MIT Press, Cambridge, MA, 1971.
9. U.F. Kocks, A.S. Argon, and M.F. Ashby: *Progr. Mater. Sci.*, 1975, vol. 19, pp. 1-271.
10. A.K. Zurek, P.S. Follansbee, and D. Kapoor: in *High Strain Rate Behavior of Refractory Metals and Alloys*, R. Asfahani, E. Chen, and A. Crowson, eds., TMS, Warrendale, PA, 1992 pp. 190-207.
11. S. Nemat-Nasser and J.B. Isaacs: *Acta Mater.*, 1997, vol. 45, pp. 907-19.
12. S. Nemat-Nasser and Y. Li: *Acta Mater.*, 1998, vol. 46, pp. 565-77.
13. A.H. Cottrell and R.J. Stokes: *Proc. R. Soc. A*, 1955, vol. 233, pp. 17-34.
14. Z.S. Basinski and J.W. Christian: *Aus. J. Phys.*, 1960, vol. 13, pp. 299-308.
15. J. Klepaczko: *Mater. Sci. Eng.*, 1975, vol. 18, pp. 121-35.
16. J.R. Klepaczko and C.Y. Chiem: *J. Mech. Phys. Solids*, 1986, vol. 34, pp. 29-54.
17. K.G. Hoge and A.K. Mukherjee: *J. Mater. Sci.*, 1977, vol. 12, pp. 1666-72.
18. M.A. Meyers, Y.J. Chen, F.D.S. Marquis, and D.S. Kim: *Metall. Mater. Trans. A*, 1995, vol. 26A, pp. 2493-2502.
19. S.R. Chen, G.T. Gray III, and S.R. Bingert: in *Tantalum. Proc. Symp. Held at 125th TMS Annual Meeting and Exhibition*, E. Chen, A. Crowson, E. Lavernia, and W. Ebihara, eds., TMS, Warrendale, PA, 1996 pp. 173-84.
20. D.J. Steinberg and C.M. Lund: *J. Appl. Phys.*, 1989, vol. 65, pp. 1528-33.
21. G.T. Gray III and K.S. Vecchio: *Metall. Mater. Trans. A*, 1995, vol. 26A, pp. 2555-64.
22. C.M. Lopatin, C.L. Wittman, J.P. Swensen, and P.F. Perron: in *High Strain Rate Behavior of Refractory Metals and Alloys*, R. Asfahani, E. Chen, and A. Crowson, eds., TMS, Warrendale, PA, 1992 pp. 241-47.
23. R.M. Davies: *Phil. Mag.*, 1948, vol. 240, p. 375.
24. H. Kolsky: *Proc. Phys. Soc, London*, 1949, vol. 62, pp. 676-700.
25. P.S. Follansbee: *Mechanical Testing, Metals Handbook*, 9th ed., ASM, Metals Park, OH, 1985, vol. 8, p. 190.
26. S. Nemat-Nasser, J.B. Isaacs, and J. E. Starrett: *Proc. R. Soc. London A*, 1991, vol. 435, pp. 371-91.
27. R. Kapoor and S. Nemat-Nasser: *Mech. Mater.* 1998, vol. 27, pp. 1-12.
28. S. Nemat-Nasser, Y. Li, and J.B. Isaacs: *Mech. Mater.*, 1994, vol. 17, pp. 111-34.
29. E. Nadgornyi: *Progr. Mater. Sci.*, 1988, vol. 31, pp. 19-21 and 232-51.
30. G. Regazzoni, U.F. Kocks, and P.S. Follansbee: *Acta Metall.*, 1987, vol. 35, pp. 2865-75.
31. G.Y. Chin and W.L. Mammel: *Trans. TMS-AIME*, 1967, vol. 239, pp. 1400-05.